Jordan Journal of Civil Engineering, Volume **19**, No. **2**, **2025**
DOI: https://doi.org/10.14525/JJCE.v19i2.05

Jordan Journal of Civil Engineering

Journal homepage: https://jjce.just.edu.jo

Numerical Investigation on Load-bearing Capacity of K-Joint Concrete-filled Steel Tube under Static Loading

Seyed Mohammad Reza Hasani [1)], ***Erfan Ashjari*** [1)], ***Masoud Mahmoudabadi*** [2)*]

[1)] *Department of Civil Engineering, Faculty of Engineering, University of Shahabe Danesh, Qom, Iran.*
[2)] *Department of Civil Engineering, Faculty of Engineering, University of Qom, Qom, Iran.*
** Corresponding Author. E-Mail: m.mahmoudabadi@qom.ac.ir*

ARTICLE INFO

Article History:
Received: 6/8/2024
Accepted: 23/2/2025

ABSTRACT

The performance of concrete-filled steel tubular (CFST) composite joints needs to be investigated under different loading types. Thus, the influential parameters should be evaluated with an aim to enhance the load-bearing capacity of structures with these composite members. This study presents a non-linear finite element modeling (FEM) analysis to evaluate the performance of K-jointed CFST joints. Accordingly, a set of 32 joint models were created using ABAQUS and the effects of various mechanical and geometrical parameters were discussed. These parameters involved steel tube thickness, section dimensions, compressive strength of infill concrete, gap and horizontal angle between joint components. Therefore, the load-bearing capacity and the stress-strain variations of K-joints were examined. Based on the results, it was noticed that by increasing the wall thickness of the primary steel tube, the initial stiffness, the ultimate load, and the displacement of the entire K-joint are reduced, but the ductility is increased. Also, as the diameter of the primary member increases, the ductility of the K-joint decreases. Furthermore, increasing the infill concrete compressive strength has a slight effect on the stress and ultimate strain of K-type joints. The failure mechanism of the joints was so that the secondary steel member is subjected to buckling at the connection point, giving rise to deformation and warping of the joint at this point, thus leading to the overall failure of the joint. It was also revealed that increasing the gap between the two secondary members significantly increases joint rigidity and reduces ductility, while it has a slight effect on the stress level of the K-joint. Moreover, the greater the angle between primary and secondary tubes, the higher the load-bearing capacity.

Keywords: Concrete-filled steel tube (CFST), K-jointed joints, Buckling; Infill concrete, Load-bearing capacity, Compressive strength.

INTRODUCTION

Today, having known the advantages of composite structures, fabricated with concrete and steel, a majority of the columns used are of composite type (Naghipour & Mehdizade, 2021). Composite columns are mainly divided into two categories: *(i)* steel columns embedded in concrete (SRC), where the steel column is placed inside the concrete section, and depending on the shape of the concrete section, the shape of the steel section can be changed (Park et al., 2013); and *(ii)* steel columns filled with concrete (CFST), in which reinforced concrete can also be used to increase the column strength. Also, the steel tube creates high stiffness and bending capacity owing to being placed at the exterior of the cross section (Gourley et al., 2001). Steel columns

with infill concrete feature advantages, including no need for framework and rebars, confining effect of peripheral steel on infill concrete, higher ductility and energy dissipation, reduction of concrete slump and creep, greater construction speed, high shear and axial strengths, and appropriate bearing capacity compared to steel columns embedded in concrete. Furthermore, the use of CFST systems can lead to 60% saving in steel consumption compared to conventional steel systems. Also, the steel tube is a permanent framework for the infill concrete, providing rebar proper allocation. By postponing the local buckling of the steel pipe, the concrete core leads to greater out-of-plane buckling than the in-plane forces. Accordingly, researchers in recent years have paid more attention to these types of elements and have proposed different solutions to improve the behavior of these columns. As a consequence, circular hollow steel (CHS) and square hollow steel (SHS) joints are widely implemented in structures like fixed and floating marine platforms, trusses with long spans, railway stations, terminals, airports, and sport stadiums. It is worth mentioning that the circular sections impose more confinement on the concrete core and the probability of local buckling is higher in square and rectangular sections. Nevertheless, square and rectangular CFST sections are still increasingly employed. Regarding CHS and SHS joints comprised of primary and secondary components, there have been several research studies, where attempts have been made to explore the effects of geometrical parameters on the performance of CFST joints. Thus, different configurations have been proposed. Among various CFST joints with different configurations are T-, Y-, and K-jointed joints. On this wise, the failure mechanism of K-joints, for instance, is attributed to the span size between braces, along with tension in one brace and compression in the other. Punching shear in the connection area and plastic deformation of the primary component are considered the most important failure modes of this type of connection (Naghipour & Hasani, 2023).

Overall, the results of the research (Yang & Tong, 2018; Thai, 2023; Yu et al., 2025; Hasani et al., 2025; Wu et al., 2025; Dong et al., 2024; Gao et al., 2024) show the superiority of CFST joints compared to reinforced concrete or steel members. Kang et al. (Kang et al., 2007) investigated the flexural behavior of a novel concrete and steel composite section to be used in bridge girders. The results indicated that tubular steel girders filled with concrete have good flexibility and maintain their strength until the end of loading. Several studies (Tomii & Sakino, 1979; Lu & Kennedy, 1994, Kilpatrick, 1997; İlgün & Sancioğlu, 2023; Alraeeini & Nikbakht, 2022; Khalaf et al., 2023; Ding et al., 2024; Du et al., 2024; Zhang et al., 2022; Le & Van Cao, 2023) have highlighted the considerable gain in flexibility of composite sections. Owing to the existence of concrete core, the failure mode of the steel tube in the compression zone changes from inward buckling to outward buckling under a far greater load-bearing capacity. Hou and Han (Hou & Han, 2017) performed a finite element analysis (FEA) of K-joints in concrete-filled double steel tube (CFDST) and CHS members. Thus, a simple relationship for calculating the strength of K-joints was proposed. It was shown that the main parameters affecting the static performance of CFDST K-joints include diameter ratio of the secondary tube to the primary one, the ratio of the radius to the thickness of the primary tube, and the properties of materials. Mashiri and Zhao (Mashiri & Zhao, 2010) investigated a T-jointed composite joint with a square cross-section. Six specimens with different geometric characteristics were prepared and the width ratio of primary section to secondary section, thickness ratio of primary section to secondary section, and thickness to width ratio of the primary section were examined. It was concluded that stress concentration at the connection point in the joints without infill concrete is higher than in those filled with concrete in the primary member. Besides, the presence of concrete reduces the stress concentration and improves joint performance. The reduction in stress concentration varied between 15% and 85%. Nassiraei et al. (Nassiraei et al., 2016) explored the performance of T- and Y-joints without infill concrete. A set of eight samples were made, four of which were strengthened with doubler plate. ABAQUS software was applied to analyze the specimens. The results showed that the diameter and thickness ratios of the secondary component to primary component have significant effects on the ultimate strength and failure modes of specimens strengthened with doubler plates. The ultimate strength of T-/Y-joint strengthened with plate under axial compression reached 270% of that of the unstrengthened joint. It was also confirmed that increasing the length and thickness of the plate improves joint strength, though the plate length has a greater effect

on strength gain than the plate thickness. Moreover, increasing the secondary member angle relative to horizon increases the ultimate strength of the joint, although at a slower rate. Wang et al. (Wang et al., 2023) experimented with the circular double skin concrete-filled steel tubes. Khalaf and Abed (Khalaf & Abed, 2023) used demolished concrete in rectangular CFSTs. Obeng and Abdullah (Obeng & Abdullah, 2022) examined the performance of reinforced CFSTs. Hu et al. (Hu et al., 2023) conducted a numerical analysis on CFST columns. Li et al. (Li et al., 2022) considered the combined effect of compression and bending in the design of CFSTs. Huang et al. (Huang et al., 2022) studied the axial behavior of CFST columns. Subedi et al. (Subedi et al., 2022) explored the response of cast-in-place CFSTs. Recently, Liao et al. (Liao et al., 2023) studied the flexural performance of novel corrugated CFDST members and were able to predict the flexural capacity of the investigated specimens. Xu et al. (Xu et al., 2022) carried out an experimental and numerical analysis on T-jointed CFST joints. In another study, Mou et al. (Mou et al., 2024) investigated the H-jointed composite CFST column joints.

Research Significance

Despite the numerous advantages of K-jointed joint, they are classified as vulnerable composite joints. These joints are typically weak at points where the secondary component is appended to the primary section. Therefore, both steel tubes are filled with concrete at the connection area in order to increase the capacity and compressive strength of the overall joint. In this research, a numerical investigation is carried out using the non-linear finite element method on the compressive strength of K-joints filled with concrete. Modeling of connections was made using ABAQUS software. Once the modeling procedure was calibrated, the effects of parameters, such as primary and secondary steel thickness of the K-joint, section dimensions of steel components, compressive strength of concrete, distance (gap) between two secondary components, and the angle between primary and secondary components, on the load-bearing capacity of the joints are discussed. Subsequently, the optimum thickness to diameter ratio for steel, compressive strength for concrete, angle between primary and secondary components, and gap between two secondary elements against loading are determined by examining the load-displacement and stress-strain diagrams of each joint specimen.

MATERIALS AND SPECIMENS

In this research, a total of 32 CFST K-joint specimens were investigated. Accordingly, 32 distinct FEM models were created to examine the impacts of geometrical parameters on the load-carrying capacity of the entire joint. In the performance evaluation of K-joints, numerical models were divided into two groups. In this regard, 16 models had infill concrete compressive strength of 30 MPa, while the other 16 models had concrete compressive strength of 45 MPa. The first group was then sub-classified into two groups with secondary tube angles of 45 and 60 degrees with respect to the primary tube chord, where there were four K-joint models in each group. Each of these four numerical models was also divided into two groups with a gap between two secondary members of values of 5mm and 7.5 mm. Based on the thickness of the primary steel tube having 2mm and 4 mm in two sub-groups, the diameter of the primary steel tube was considered 110mm and 120 mm. The geometric properties of a model joint are illustrated in Figure (1). Also, Table 1 reports all the model specifications studied in this paper.

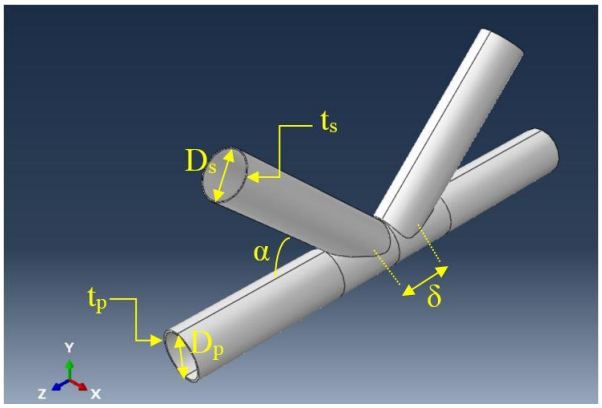

Figure (1): The geometric properties of K-joint model in ABAQUS

Table 1. Properties of K-joints modeled in ABAQUS

No.	K-joint ID	Concrete compressive strength f_c (MPa)	Horizontal angle α (°)	Secondary members gap δ (mm)	Primary tube thickness t_p (mm)	Secondary tube thickness t_s (mm)	Primary tube diameter D_p (mm)	Secondary tube diameter D_s (mm)
1	F30-45-05-02-110	30	45	05	04	02	110	110
2	F30-45-05-02-120	30	45	05	04	02	120	110
3	F30-45-05-04-110	30	45	05	04	04	110	110
4	F30-45-05-04-120	30	45	05	04	04	120	110
5	F30-45-7.5-02-110	30	45	7.5	04	02	110	110
6	F30-45-7.5-02-120	30	45	7.5	04	02	120	110
7	F30-45-7.5-04-110	30	45	7.5	04	04	110	110
8	F30-45-7.5-04-120	30	45	7.5	04	04	120	110
9	F30-60-05-02-110	30	60	05	04	02	110	110
10	F30-60-05-02-120	30	60	05	04	02	120	110
11	F30-60-05-04-110	30	60	05	04	04	110	110
12	F30-60-05-04-120	30	60	05	04	04	120	110
13	F30-60-7.5-02-110	30	60	7.5	04	02	110	110
14	F30-60-7.5-02-120	30	60	7.5	04	02	120	110
15	F30-60-7.5-04-110	30	60	7.5	04	04	110	110
16	F30-60-7.5-04-120	30	60	7.5	04	04	120	110
17	F45-45-05-02-110	45	45	05	04	02	110	110
18	F45-45-05-02-120	45	45	05	04	02	120	110
19	F45-45-05-04-110	45	45	05	04	04	110	110
20	F45-45-05-04-120	45	45	05	04	04	120	110
21	F45-45-7.5-02-110	45	45	7.5	04	02	110	110
22	F45-45-7.5-02-120	45	45	7.5	04	02	120	110
23	F45-45-7.5-04-110	45	45	7.5	04	04	110	110
24	F45-45-7.5-04-120	45	45	7.5	04	04	120	110
25	F45-60-05-02-110	45	60	05	04	02	110	110
26	F45-60-05-02-120	45	60	05	04	02	120	110
27	F45-60-05-04-110	45	60	05	04	04	110	110
28	F45-60-05-04-120	45	60	05	04	04	120	110
29	F45-60-7.5-02-110	45	60	7.5	04	02	110	110
30	F45-60-7.5-02-120	45	60	7.5	04	02	120	110
31	F45-60-7.5-04-110	45	60	7.5	04	04	110	110
32	F45-60-7.5-04-120	45	60	7.5	04	04	120	110

It should be noted that the notation of the specimens was designated based on the model properties. For example, the numerical model F30-60-05-02-120 represents a specimen with filler concrete with a 28-day cylindrical compressive strength equal to 30 MPa, a horizontal angle of 60 degrees, a gap between two secondary members of 5 mm, primary steel thickness and diameter of 2mm and 120 mm, respectively. The primary tube thickness and the secondary tube diameter are kept constant at all models, being 4mm and 110 mm, respectively. During the modeling process, steel sections with a yield stress of 360 MPa and an elastic modulus of 210000 MPa were used. Also, a density of 7850 kg/m^3, a plastic strain of 0.2, and a Poisson's ratio of 0.3 were considered for the steel sections. Besides, for concrete sections, a Poisson's ratio of 0.2 and a density of 2400 kg/m^3 were applied. Also, the Young's modulus of concrete with compressive strengths of 30 MPa and 45 MPa was chosen as 26070 MPa and 30103 MPa, respectively.

RESEARCH METHODOLOGY

Numerical methods are alternative approaches to experimentations in providing solutions to problems at different conditions. In this study, FEA was conducted

using ABAQUS to evaluate the effects of mechanical and geometrical parameters on the performance of K-joints. Thus, static analysis was implemented in the modeling process. Different models have been proposed in the literature regarding the definition of materials including elastic-plastic, elastic-perfectly plastic, linear hardening, and multi-linear hardening materials. In this investigation, the ST37 tubular steel features elastic-plastic model with a strain-hardening modulus of $0.005E_s$, where E_s is the steel modulus of elasticity. Also, rigid steel plates having a Poisson's ratio of 0.3 and a Young's modulus of 1000 GPa were modeled at supports and loading points in order to prevent deformations. Also, concrete material behavior was assumed as elastic isotropic. The steel-concrete contact was specified as a hard contact along the normal direction. Additionally, Mohr-Coulomb friction was defined along the vertical direction by smearing surface-to-surface contact. Thereby, a couple of master-slave surfaces, with concrete being slave and the steel tube being master. This was carried out, because concrete is softer and its mesh is finer compared to steel. Hence, the margin of error would be moderated. A relative slip was allowed between surface couples in the friction model. Thus, the shear force is estimated *via* friction coefficient and tangential pressure. The penalty friction formulation having a coefficient of 0.25 between steel and concrete was considered, according to Ellobody and Young (Ellobody & Young, 2006). Concrete, supports, and loading plates were defined in ABAQUS with 8-node solid elements with reduced integration pattern. Moreover, tubular steel sections were introduced to the software with 4-node shell elements. Figure (2-a) demonstrates mesh configuration of an example K- joint in this study. The mesh convergence was performed to obtain an appropriate meshing size, such that allowable estimates with low computational time would be achieved. Consequently, local seeds with single bias having a minimum size of 5 mm and an approximate global size of 25 mm were applied in the meshing process. The boundary conditions of the K-joint were simply-supported areas. A uniform horizontal pressure load of 200 kN was applied to the primary steel tube. The deformation of the loading rigid block plate could be ignored due to its large stiffness. Figure (2-b) depicts K-joint boundary conditions and the entire loading setup.

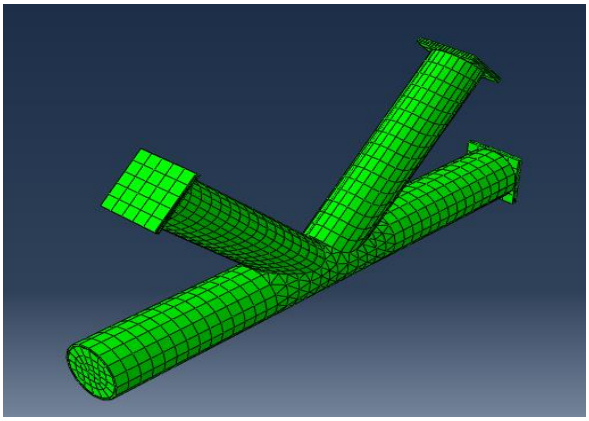

(a). The mesh configuration of K-joint model in ABAQUS

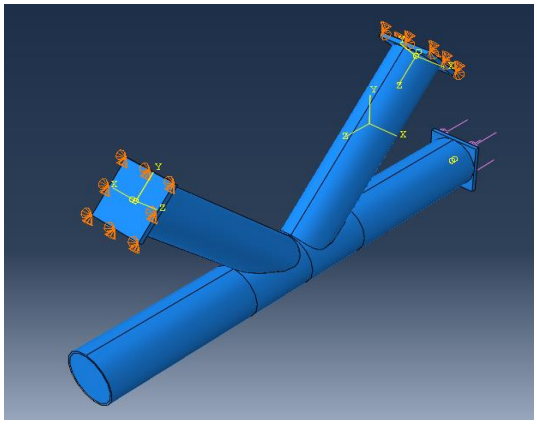

(b). The loading setup and boundary conditions of K-joint model in ABAQUS

Figure (2): The mesh configuration and loading setup and boundary conditions of K-joint model in ABAQUS

Validation of FEM

Based on the modeling output, the FEM was validated with the experimental results reported by Hasani et al. (Hasani et al., 2025). Figure (3) compares the K-joint buckling mode in the FEM approach in the present study with experimental and FEM models of Hasani et al. (Hasani et al., 2025). It can be seen that the overall joint response, particularly in predicting the warping section of the joint, is in good agreement, which shows the accuracy of the modeling process.

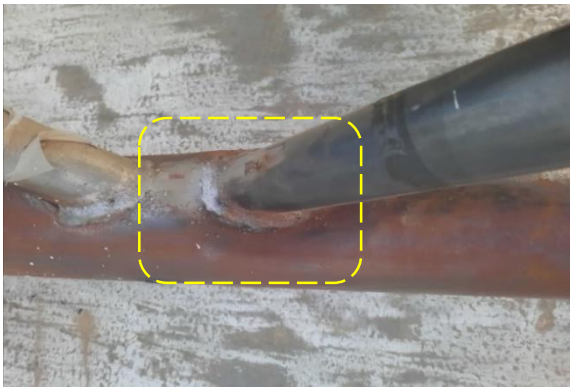

(a)

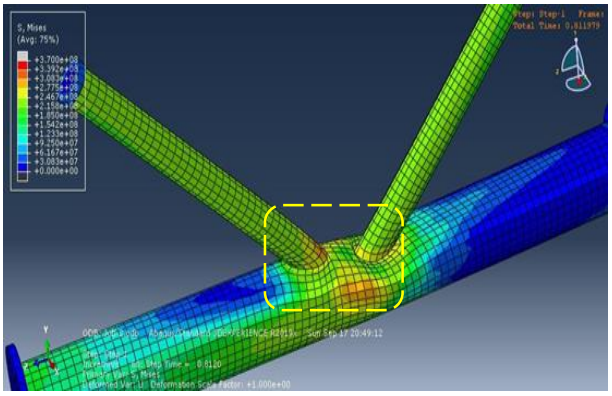

(b)

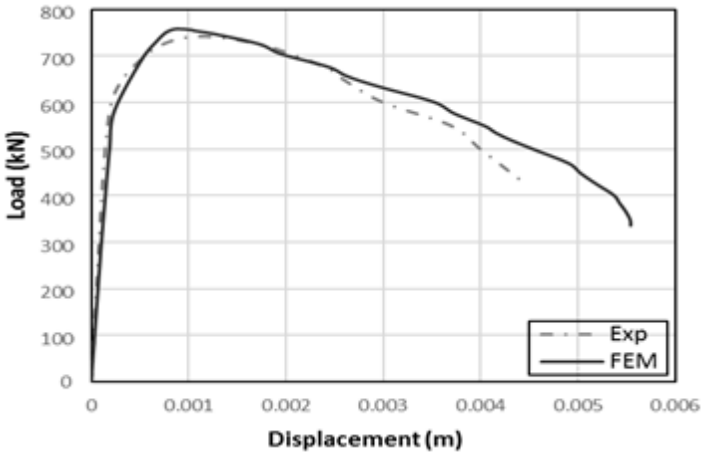

(c)

Figure (3): Validation of (a) joint FEM in this study with (b) experimental results of Hasani et al. (Hasani et al., 2025) and (c) Validation of FEM and experimental results

RESULTS AND DISCUSSION

In this section, the results of the numerical models are presented. A parametric study was performed on the performance of K-joints under static loading. The effects of varying parameters, like infill concrete compressive strength, distance and angle between two secondary members, thickness and diameter of primary and secondary steel tubes, on the overall strength of the K-joints in terms of load-displacement and stress-strain diagrams are discussed. In this regard, a sample stress distribution contour of specimen F30-45-05-02-120 is shown in Figure (4). Based on this figure, the warping and the deformation of the entire joint can be observed.

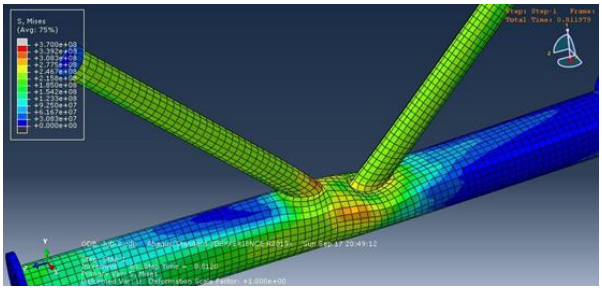

Figure (4): Mises stress distribution of the K-joint model F30-45-05-02-120

Subsequently, Figure (5-a) shows the load-displacement diagram of the joint specimen F30-45-05-02-110. As can be seen in the figure, load surges with increasing the displacement up to 0.79 mm, after which

the stiffness of the joint is markedly reduced, and thus, the slope of the load-displacement diagram decreases. The load corresponding to this point is equal to 263 kN. The reason for this issue can be attributed to the fact that with the gradual increase in load, the secondary steel member sustains buckling, suffering high pressure at the connection point, where the secondary member attaches the primary tube. This issue causes the deformation and warping of this area of the K-joint assembly. With increasing load, the connection point undergoes failure and the load-carrying capacity is critically reduced. The ultimate load in this specimen is 392 kN and the corresponding displacement is 14.34 mm. Furthermore, the stress-strain curve of specimen F30-45-05-02-110 is shown in Figure (5-b). Based on this figure, the failure point of the K-joint is equivalent to the stress of 265 MPa and the corresponding strain of 0.025. According to the linear part of the diagram, the joint maintains its stiffness at first, until its stiffness is reduced due to the buckling of the secondary steel member, leading to the overall failure of the K-joint.

In a similar manner, Figure (5-a) represents the load-displacement diagram of specimen F30-45-05-02-120. According to this figure, the rising section of the curve continues up to a horizontal load of 265 kN and a displacement of 0.72 mm. Then, as in the previous model, the slope is reduced and the stiffness of the connection is reduced due to the buckling in the steel member. According to the load-displacement diagram of this model, the specimen fails at an ultimate load of 385 kN and an expected displacement of 13.71 mm. This is indicative of the fact that increasing the primary tube thickness leads to a decrease in the ultimate load and displacement of the entire K-joint. In addition, the stress-strain diagram of specimen F30-45-05-02-120 is shown in Figure (5-b). According to this figure, the failure point of the K-joint is equivalent to the stress of 259 MPa, where the equivalent point of strain is 0.019. According to this diagram, the failure strain has decreased compared to the specimen with a smaller primary tube diameter; i.e., the model with a diameter of 110 mm. This issue reflects the fact that the ductility of the K-joint decreases as the diameter of the main member increases. Therefore, the joint maintains its stiffness at first, until its stiffness is reduced under the buckling of the secondary steel member, and this leads to the complete failure of the K-joint.

By increasing the wall thickness of the primary steel tube from 2 mm to 4 mm, it can be seen that the initial stiffness of the connection is reduced and its ductility is increased. According to Figure (5-a), the maximum load in the K-joint is 398 kN and the equivalent displacement is 0.67 mm, where the joint fails at this point. Also, the stress-strain diagram of joint F30-45-05-04-110 is shown in Figure (5-b). According to this figure, the failure point of the connection happens at a stress of 230 MPa and a strain of 0.001. According to the linear section of the diagram, the joint maintains its stiffness until the buckling of the steel members, resulting in the total failure of the K-joint. By increasing the diameter of the primary member from 110 mm to 120 mm, it can be seen that the initial stiffness of the connection is reduced and its ductility is increased. According to Figure (5-a), the maximum load on this joint is 398 kN and the equivalent displacement is 0.96 mm. Figure (5-b) demonstrates variations of stress against strain in K-joint model F30-45-05-04-120. Thus, failure occurs at a stress of 230 MPa and a strain of 0.0009. These values are equal in stress, but lower in strain, when compared to joint model F30-45-05-04-110.

In examining the response of numerical models with a gap of δ=7.5 mm between two secondary members, Figure (5-a) presents changes in the horizontal load on the joint compared to horizontal displacement. According to this figure, it can be concluded that the maximum bearing capacity of the K-joint F30-45-7.5-02-110 is equal to 393 kN and the displacement is 14.77 mm. These values, when compared to those of model F30-45-05-02-110, in which the gap between the two secondary members is equal to 5 mm, show no changes in load capacity and a 2% increase in displacement. In a similar way, Figure (5-b) shows the stress changes in connection *versus* strains induced in the joint member. It can be seen in this figure that the maximum stress in model F30-45-7.5-02-110 is 264 MPa and the strain is 0.24 mm. By comparing these values with those of specimen F30-45-05-02-110 with a gap of 5 mm between two secondary members, it can be seen that the amount of stress is decreased by 1% and the strain corresponding to failure stress is slashed by 4%. This is indicative of the important result that increasing the gap between the two secondary members reduces the ductility of K-joints, while it has a slight effect on the stresses in these types of connection. Figure (5-a) depicts load-displacement changes of model F30-45-7.5-02-120. Accordingly, the maximum load in the

connection is 378 kN and the corresponding displacement is 13.16 mm. Compared to the same model (model with a gap of 5 mm), these values show a reduction of 2% in load-carrying capacity and 4% in displacement. The reason for such decrease is actually the increase of the gap between the two secondary members by 50%, which leads to a drop in the bearing capacity of the K-joint. In Figure (5-b), the stress-strain diagram of model F30-45-7.5-02-120 is given. According to this figure, the failure stress is equal to 262 MPa and the corresponding strain is equal to 0.022.

The curves in Figure (5-a) are plotted in order to compare load-displacement variations in different K-joints, as to when changing the investigated mechanical and geometric parameters. Similarly, to compare the stress capacity with respect to changes in the investigated parameters, Figure (5-b) demonstrates stress-strain diagrams. Based on the comparative curves in Figure (5-a), it can be inferred that the joint specimen F30-45-7.5-04-120 has the highest load capacity and the lowest displacements. In the same way, the model specimen F30-45-7.5-02-110 has the lowest load-bearing capacity and the highest displacement among the examined models having a horizontal angle of α=45°. This observation indicates that both the gap and the diameter of the primary member are influential in the bearing capacity of K-jointed connections. The stress-strain diagrams of the investigated K-joints with an angle of α=45° show that specimen F30-45-7.5-04-120 has the lowest amount of ductility capacity, and thus, a brittle failure mode. In contrast, model F30-45-5-02-110 has the highest ductility and failure strain. With the change in horizontal angle of the secondary members from α=45° to α=60°, the behavior of load changes against horizontal displacement and the stress-strain diagram of K-joints filled with concrete with a 28-day compressive strength of 30 MPa were investigated in this research. It is seen in diagrams with α=60° that the process of load and stress variations is almost similar to specimen models with a horizontal angle of α=45°, though with different values. In order to compare the changes with respect to parameters, such as the diameter and wall thickness of the primary member, Figure (5-c) is presented. Also, to compare the stress capacity with respect to changes in the investigated parameters, Figure (5-d) shows stress-strain diagrams. According to the comparative curves in Figure (5-c), it can be seen that model F30-60-7.5-02-110 has the highest displacement among the examined K- joints. The reason for this can be associated with the higher gap between the two secondary members, the lower wall thickness of the primary member, and the smaller diameter of the primary member. In this figure, the ductility of the K-joint is reduced and the connection becomes more rigid by increasing the amount of gap between two sub-members. By comparing the stress-strain results of the joints modeled in the ABAQUS software presented in Figure (5-d), the important result can be realized that model F30-60-7.5-02-110 has the highest strain capacity, and the stress values in this model are higher than in the other K-joints.

This study also examines the load-displacement behavior of steel K-joints with a 28-day infill concrete compressive strength of 45 MPa. In this regard, Figure (6-a) shows the load-displacement diagram of joint F45-60-05-02-110. As can be seen in the figure, the amount of load takes an increasing course with the increase in displacement until the displacement reaches 0.97 mm. Then, the capacity of the joint is strongly reduced and the load-displacement diagram slope decreases. The load equivalent to this point is equal to 282 kN. In relation to the cause of this issue, it can be concluded that the secondary steel member is subjected to buckling with the gradual increase of the exerted load, and thus, undergoes pressure at the connection point of secondary member with the primary element. As a result, this issue causes deformation and warping of this part of the connection. With the increase of the induced load, the connection starts to fail and its load-carrying capacity is greatly reduced. In addition, the stress-strain diagram of specimen F45-45-05-02-110 is shown in Figure (6-b). According to this figure, the failure point of the K-joint is equivalent to the stress of 259 MPa and the corresponding strain of 0.019. According to the linear part of the diagram, the joint maintains its stiffness at first, until its stiffness is reduced due to the buckling of the secondary steel member, leading to the overall failure of the K-joint. An interesting point to note in this model is that compared to the similar model with a concrete compressive strength of 30 MPa (model F30-45-05-02-110), the amount of failure stress is reduced by 2% and the corresponding strain at the corresponding point is reduced by 24%. Figure (6-a) shows the load-displacement diagram of specimen F45-45-05-02-120. According to this figure, the rising section of the curve continues up to a horizontal load of 241 kN and a

displacement of 0.53 mm. Then, as in the previous model, the slope is reduced and the stiffness of the connection is reduced due to the buckling in the steel member. According to the load-displacement diagram of this model, the specimen fails at an ultimate load of 323 kN and an expected displacement of 1.83 mm. This is indicative of the fact that increasing the primary tube thickness leads to a decrease in the ultimate load and displacement of the entire K-joint. In addition, the stress-strain diagram of specimen F45-45-05-02-120 is illustrated in Figure (6-b). Based on this diagram, the failure point of the K-joint is equivalent to the stress of 241 MPa, where the equivalent point of strain is 0.0022. According to this diagram, the failure strain has decreased compared to the specimen with a smaller primary tube diameter; i.e. the model with a diameter of 110 mm. This issue reflects the fact that the ductility of the K-joint decreases as the diameter of the primary member increases. Therefore, the joint maintains its stiffness at first, until its stiffness is reduced under the buckling of the secondary steel member, and this leads to the complete failure of the joint.

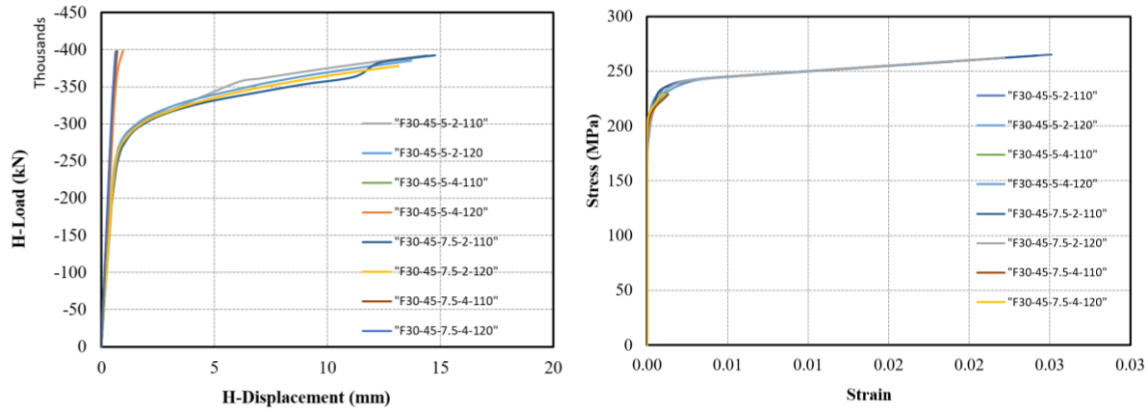

(a) Comparative load-displacement curves for K-joint specimens with α=45°

(b) Comparative stress-strain curves for K-joint specimens with α=45°

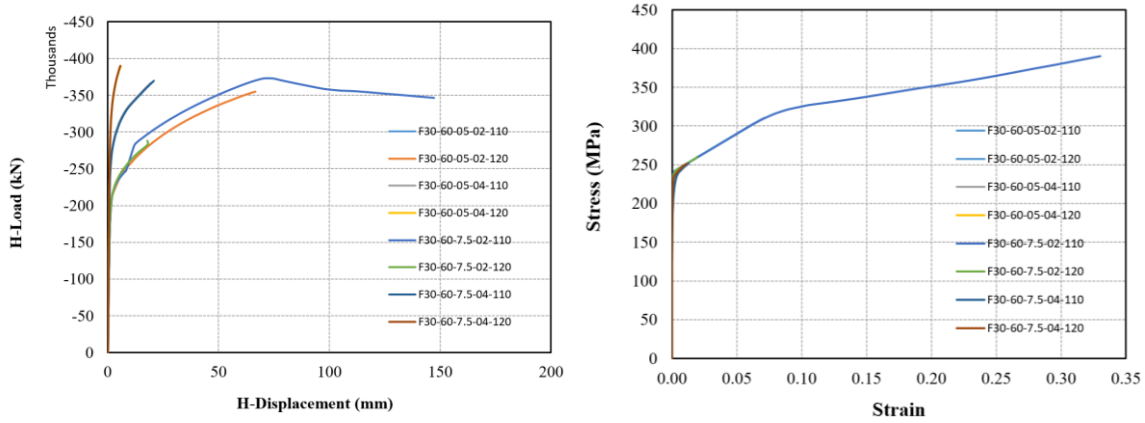

(c) Comparative load-displacement curves for K-joint specimens with α=60°

(d) Comparative stress-strain curves for K-joint specimens with α=60°

Figure (5): Comparative load-displacement and stress-strain curves for K-joint specimens with α=45° and α=60°

It can be seen, by increasing the wall thickness of the primary steel tube from 2 mm to 4 mm, that the initial stiffness of connection F45-45-05-04-110 is reduced and its ductility is increased. According to Figure (6-a), the maximum load in the K-joint is 397 kN and the equivalent displacement is 0.62 mm, where the joint fails at this point. Correspondingly, the stress-strain diagram of joint F45-45-05-04-110 is shown in Figure (6-b). Based on this figure, the failure point of the connection happens at a stress of 231 MPa and a strain of 0.0015. According to the linear section of the diagram, the joint maintains its stiffness until the buckling of the steel members, resulting in the total failure of the K-joint. At the same time as the diameter of the primary member increases from 110 mm to 120 mm, the initial stiffness of the joint decreases and its

ductility increases. Noticing Figure (6-a), the maximum load on the K-joint specimen is 398 kN and the equivalent displacement is 0.91 mm, the displacement at which connection F45-45-05-04-110 fails. Figure (6-b) shows variations of stress against strain in K-joint model F45-45-05-04-120. Thus, failure occurs at a stress of 229 MPa and a strain of 0.0008. These values are equal in stress, but lower in strain, when compared to joint model F30-45-05-04-110. Therefore, it can be concluded that the increase in strength of the infill concrete does not have much effect on the stress and failure strain of the K-jointed joints.

In investigating the behavior of models with a gap of δ=7.5 mm between two secondary members, Figure (6-a) shows changes in the horizontal load on the joint compared to horizontal displacement. According to this figure, it can be concluded that the maximum bearing capacity of the K-joint F45-45-7.5-02-110 is equal to 378 kN and the displacement is 10.75 mm. These values, when compared to model F45-45-05-02-110, in which the gap between the two secondary members is equal to 5 mm, show an increase of 1% in load-carrying capacity and 4% in the displacement capacity. In addition, Figure (6-b) reflects the stress variations in connection versus strains induced in the joint member. It can be seen in this figure that the maximum stress in model F45-45-7.5-02-110 is 258 MPa and the strain is 0.018. By comparing these values with those of specimen F45-45-05-02-110 with a gap of 5 mm between the two secondary members, it can be seen that the amount of stress is decreased by 1% and the strain corresponding to failure stress is slashed by 5%. This is indicative of the important result that increasing the gap between the two secondary members reduces the ductility of K-joints, while it has a slight effect on the stresses in these types of connection. According to Figure (6-a), the diagram of load-displacement changes of joint F45-45-7.5-02-120 is shown. Thus, the maximum load in the connection is 397 kN and the corresponding displacement is 12.26 mm. Compared to the same model (model F45-45-05-02-120 with a gap of 5 mm), these values show a reduction of 19% in load-carrying capacity and 85% in displacement. The reason for such decrease is actually the increase of the gap between the two secondary members by 50%, which leads to a drop in the bearing capacity of the K-joint. In Figure (6-b), the stress-strain diagram of model F45-45-7.5-02-120 is given. According to this figure, the failure stress is equal to 234 MPa and the corresponding strain is equal to 0.014. The noteworthy point in comparing this model with a similar specimen with the same specifications and the only difference in the 28-day compressive strength of 30 MPa is that the stress decreases by 11% and the equivalent strain by 36%, as the compressive strength of concrete is increased.

In order to compare the load-displacement variations in different K-joints, the curves in Figure (6-a) are plotted, as to when changing the investigated mechanical and geometric parameters. Also, to compare the stress capacity with respect to changes in the investigated parameters, Figure (6-b) demonstrates stress-strain diagrams. Based on the comparative curves in Figure (6-a), it can be inferred that the joint specimen F45-45-7.5-04-120 has the highest load capacity and the lowest displacement. It can be said that this model has shown the best performance among other examined specimens. In the same way, the model specimen F45-45-7.5-02-110 has the lowest load-bearing capacity and the highest displacement among the examined models having a horizontal angle of α=45°. This observation indicates that both the gap and the diameter of the primary member are influential in the bearing capacity of K-jointed connections. Subsequently, the stress-strain diagrams of the investigated K-joints with an angle of α=45° show that the two specimens F45-45-5-04-120 and F45-45-7.5-02-110 have the lowest amount of ductility capacity, and thus, a brittle failure mode. On the other hand, F30-45-5-02-110 and F30-45-7.5-02-110 have the highest ductility and failure strain, respectively. This is consistent with the results of the previous discussion regarding K-joints filled with 30-MPa concrete. In the present research, together with the change in horizontal angle of the secondary members from α=45° to α=60°, the behavior of load changes against horizontal displacement as well as the stress-strain diagram of K-joints filled with concrete with a 28-day compressive strength of 45 MPa were investigated. It is seen in diagrams with α=60° that the process of load and stress variations is almost similar to that of specimen models with a horizontal angle of α=45°, though with different values. In order to compare the changes with respect to parameters such as the diameter and wall thickness of the primary member, Figure (6-c) is presented. Also, to compare the stress capacity with respect to changes in the investigated parameters, Figure (6-d) shows stress-strain diagrams. According to the

comparative curves in Figure (6-c), it can be seen that models F45-60-7.5-02-120 and F45-60-7.5-04-120 have the highest displacement and ductility among the examined K- joints. This observation can be due to various reasons, such as the increase in the gap between the two secondary members, the wall thickness and the diameter of the primary member. Therefore, it is clearly understood that the specimens with a gap of δ=7.5 mm between two secondary members have the best results regarding the bearing capacity and ductility. In addition, it is noted in this figure that the model F45-60-05-04-120 has the highest connection stiffness and the lowest ductility. This is because the gap distance between two secondary members has a significant impact on the rigidity of the K-joint and its ductility. Similarly, by comparing the stress-strain results of the joints modeled in the ABAQUS software presented in Figure (6-d), it can be concluded that specimens F45-60-7.5-02-120 and F45-60-7.5-04-120 have the best response with a slight difference, and the stress and failure strain of these two models are higher than those of the other K-joints. Therefore, it can be concluded that the gap between two secondary members has a pronounced effect on the stress-strain behavior of the connection, thus enhancing the ductility in combination with the diameter and thickness of the primary joint member.

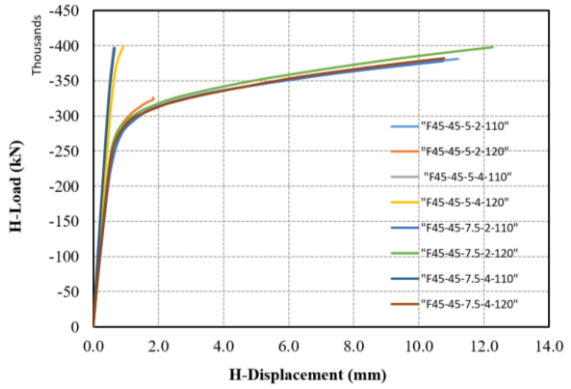

(a) Comparative load-displacement curves for K-joint specimens with α=45°

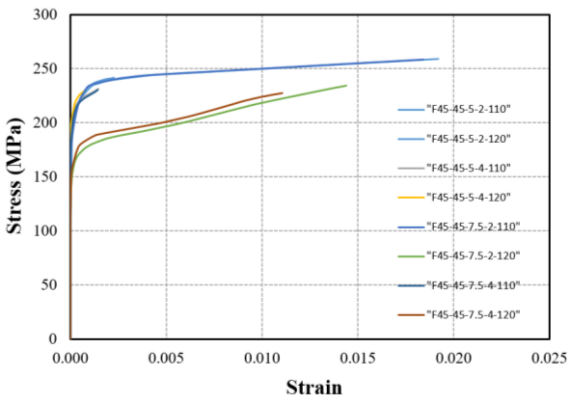

(b) Comparative stress-strain curves for K-joint specimens with α=45°

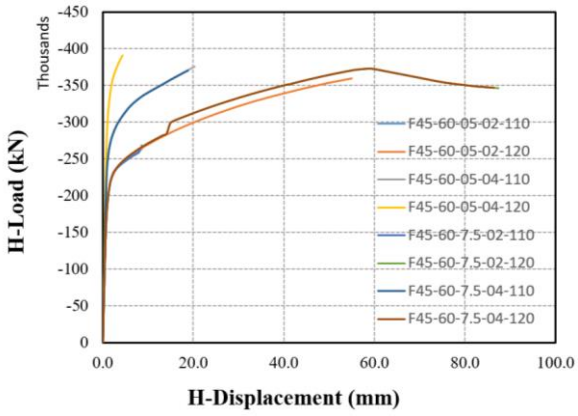

(c) Comparative load-displacement curves for K-joint specimens with α=60°

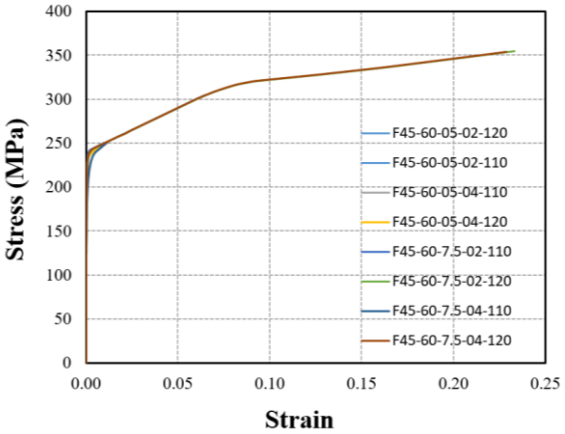

(d) Comparative stress-strain curves for K-joint specimens with α=60°

Figure (6): Comparative load-displacement and stress-strain curves for K-joint specimens with α=45° and α=60°

CONCLUSIONS

In the present study, the numerical investigation was carried out on the load-displacement behavior and stress-strain changes of K-jointed joints filled with concrete under static loading. Therefore, various parameters, such as variations in the horizontal angle and the amount of gap between the two secondary members, the diameter and thickness of the primary member, as well as the 28-day compressive strength of

the infill concrete, were investigated. According to the obtained results, the following conclusions can be drawn:

- As loading is gradually increased on K-joints, the secondary steel member is subjected to buckling at the connection point. This gives rise to deformation and warping of the joint at this point, leading to the overall failure of the joint.
- By increasing the wall thickness of the primary steel tube, the initial stiffness, the ultimate load, and displacement of the entire K-joint are reduced, but the ductility is increased. Also, as the diameter of the primary member increases, the ductility of the K-joint decreases.
- Increasing the infill concrete compressive strength has a slight effect on the stress and ultimate strain of K-type joints.
- Increasing the gap between the two secondary members significantly increases joint rigidity and reduces ductility, while it has a slight effect on the stress of the K-joint. In this respect, raising the gap by 50% results in a reduction of 2% in the load-carrying capacity and 4% in the displacement.
- The trend of load variations *versus* the horizontal displacement as well as the stress-strain behavior of K-joints with a horizontal angle of α=45° is almost similar to that of α=60°, though the response values are higher. Thus, the greater the angle between primary and secondary tubes, the higher the load-bearing capacity.

Data Availability

There is no data available for our manuscript.

REFERENCES

Alraeeini, A.S., and Nikbakht, E. (2022, October). "Corrosion effect on the flexural behaviour of concrete filled steel tubulars with single and double skins using engineered cementitious composite". In: Structures, 44, 1680-1694. Elsevier.

Ding, F.X., Sadat, S.I., Lyu, F., and Yin, Y. (2024). "Flexural performance of rectangular CFST composite T-beams: Experimental, numerical, and theoretical investigation". Journal of Constructional Steel Research, 213, 108356.

Dong, J., Zheng, S., Zhang, Z., Liu, H., and Li, Y. (2024). "Experimental study on seismic performance of RC beam-CFST column joint combination using ECC". Engineering Structures, 312, 118188.

Du, Y., Gao, D., Chen, Z., Deng, X.F., and Qian, K. (2023). "Experimental study on the flexural behavior of square high-strength concrete-filled steel tube beams with different CFRP wrapping schemes". Composite Structures, 304, 116325.

Ellobody, E., Young, B., and Lam, D. (2006). "Behaviour of normal and high strength concrete-filled compact steel tube circular stub columns". Journal of Constructional Steel Research, 62 (7), 706-715.

Gao, C., Wang, J., Wang, Y., and Wei, W. (2024). "Behaviour of concrete-filled circular steel tubular K-joints in wind turbine towers". Journal of Constructional Steel Research, 218, 108694.

Gourley, B.C., Tort, C., Hajjar, J.F., and Schiller, P.H. (2001). "A synopsis of studies of the monotonic and cyclic behaviour of concrete-filled steel tube beam-columns". Minneapolis: University of Minnesota.

Hasani, S.M.R., Naghipour, M., and Nematzadeh, M. (2025). "Effect of geometric parameters on ultimate strength of axially-loaded CFDST chord to CFST brace K-joints". Marine Structures, 102, 103780.

Hou, C., and Han, L. H. (2017). "Analytical behaviour of CFDST chord to CHS brace composite K-joints". Journal of Constructional Steel Research, 128, 618-632.

Hu, X., Albareda, A., Bu, X., and López-Almansa, F. (2023). "Numerical analysis of the axial-flexural behavior of CFST columns with active transverse pre-stressing". Buildings, 13 (10), 2411.

Huang, Y., Li, W., Lu, Y., Liang, H., and Yan, Y. (2022). "Behaviour of CFST slender columns strengthened with steel tube and sandwiched concrete jackets under axial loading". Journal of Building Engineering, 45, 103613.

İlgün, A., and Sancioğlu, S. (2023). "Flexural behaviour of different CFST cross-section shapes with the same steel cross-sectional area". Sādhanā, 48(2), 53.

Kang, J.Y., Choi, E.S., Chin, W.J., and Lee, J.W. (2007). "Flexural behavior of concrete-filled steel tube members and its application". Steel Structures, 7 (4), 319-324.

Khalaf, S., and Abed, F. (2023). "The use of demolished concrete lumps (DCLs) in Rectangular CFSTs under flexure.

Khalaf, S., Abed, F., and Alhoubi, Y. (2023). "Flexural behavior of circular concrete filled steel tubes with partially incorporated demolished concrete lumps". Composites Part C: Open Access, 10, 100346.

Kilpatrick, A.E. (1997). "Tests on high-strength composite concrete columns". School of Civil Engineering, Curtin University of Technology.

Le, K.B., and van Cao, V. (2023). "Flexural behavior and reliability analysis of rectangular concrete-filled cold-formed steel tabular beams". Journal of Constructional Steel Research, 211, 108173.

Li, G., Hou, C., and Shen, L. (2022). "Combined compression-bending performance and design of CFSTs with localised pitting corrosion". Journal of Constructional Steel Research, 192, 107247.

Liao, X., Li, X., Li, Z. W., Li, C.Z., and Zhong, T. (2023, June). "Flexural behavior of novel CFDST components with external welded corrugated steel tubes". In: Structures, 52, 42-56. Elsevier.

Lu, Y.Q., and Kennedy, D.L. (1994). "The flexural behaviour of concrete-filled hollow structural sections". Canadian Journal of Civil Engineering, 21 (1), 111-130.

Mashiri, F.R., and Zhao, X.L. (2010). "Square hollow section (SHS) T-joints with concrete-filled chords subjected to in-plane fatigue loading in the brace. Thin-Walled Structures, 48 (2), 150-158.

Mou, B., Yan, X., Yu, Y., and Wang, Z. (2024). "Composite CFST column to H-shaped steel beam joint: Experimental and numerical investigation". Engineering Structures, 299, 117083.

Naghipour, M., and Hasani, S.M.R. (2024). "Numerical investigation of ultimate bearing capacity of circular and square concrete-filled double steel tubular T-joints". Proceedings of the Institution of Mechanical Engineers, Part L: Journal of Materials: Design and Applications, 238 (6), 1099-1113.

Naghipour, M., and Mehdizade, M. (2021). "Effect of strengthening and infill concrete on bending behavior of Y- and T-shape connections". Iranian Journal of Marine Technology, 7 (4), 43-57.

Nassiraei, H., Lotfollahi-Yaghin, M.A., and Ahmadi, H. (2016). "Static strength of collar plate reinforced tubular T/Y-joints under brace compressive loading". Journal of Constructional Steel Research, 119, 39-49.

Obeng, N.S., and Abdullah, A.A. (2022). "Flexural behaviour of rectangular CFST beams strengthened with innovative steel plate reinforcements". Journal of Engineering Science and Technology, 17 (6), 4320-4334.

Park, H.S., Kwon, B., Shin, Y., Kim, Y., Hong, T., and Choi, S.W. (2013). "Cost and CO_2 emission optimization of steel reinforced concrete columns in high-rise buildings". Energies, 6 (11), 5609-5624.

Subedi, N., Thusoo, S., Obara, T., Kono, S., Kaneko, O., Hayakawa, T., …, and Mukai, T. (2022). "Flexural performance of cast-in-place concrete-filled steel tube piles under varying axial load". Thin-Walled Structures, 174, 109130.

Thai, H.T. (2024, October). "Beam-to-CFST column joints in steel-concrete composite buildings: A comprehensive review". In: Structures, 68, 107123. Elsevier.

Tomii, M., and Sakino, K. (1979). "Experimental studies on the ultimate moment of concrete filled square steel tubular beam-columns". Transactions of the Architectural Institute of Japan, 275, 55-65.

Wang, F., Cheng, Z., and Shen, J. (2023). "Flexural fatigue behavior of butt-welded circular concrete-filled double skin steel tube (CFDST): Experimental study and numerical modeling". Marine Structures, 88, 103380.

Wu, Q., Luo, J., Chen, K., Han, D., and Zheng, Q. (2025). "Fatigue performance and SCF-calculation method of CFST K-Joints with array-arranged and circular-arranged internal studs". Journal of Structural Engineering, 151(4), 04025010.

Xu, X., Cheng, R., Yang, P., and Yu, Y. (2022). "Experimental and numerical investigations on square CFST column to U-shaped steel-concrete composite beam joints with internal T-shaped diaphragms". Journal of Building Engineering, 60, 105172.

Yang, D., and Tong, L. (2018). "Research on hot spot stress calculation method of CHS-CFSHS joints". Jordan Journal of Civil Engineering, 12 (2).

Yu, P., Guo, Z., Yun, W., and Guo, X. (2025, February). "Investigation on the new bolt-welded joint of concrete-encased CFST under eccentric compression". In: Structures, 72, 108183. Elsevier.

Zhang, Z.Y., Sun, Q., Wang, J.Q., Zhao, C., Zhao, B.Z., and Wang, J.T. (2022). "Experimental and analytical research on flexural behavior of concrete-filled high-strength steel tubular members". Materials, 15 (11), 3790.